To be submitted to the Astrophysical Journal
Preprint typeset using LaTeX style emulateapj v. 12/16/11

DETECTION OF UNIVERSALITY OF DARK MATTER PROFILE FROM SUBARU WEAK LENSING MEASUREMENTS OF 50 MASSIVE CLUSTERS

Hiroko Niikura[1,2], Masahiro Takada[1], ...
[1] Kavli Institute for the Physics and Mathematics of the Universe (WPI), TODIAS, The University of Tokyo, Chiba, 277-8583, Japan
[2] Physics Department, The University of Tokyo, Bunkyo, Tokyo 113-0031, Japan
To be submitted to the Astrophysical Journal

ABSTRACT

TBD

1. INTRODUCTION

2. TRANSIENTS OF HYPER SUPRIME-CAM DATA

In this study we propose a transient search for M31 dense-star region, using Hyper Suprime-Cam at Subaru telescope. Hyper Suprime-Cam (HSC) is a wide-field imaging camera attached at the prime focus of Subaru telescope. This camera consists of 116 CCD chips; 104 for science, 4 for auto-guide, and 8 for auto-focus, and each CCD has 2k x 4k pixels, with a pixel scale of 0.168 arcsec. One unique characteristic of this camera is the wide field of view (FoV) as large as 1.5 degree at a single frame, which is three times larger than the size of full Moon in radius. Also high resolution is expected owing to the large primary mirror of 8.2 meters in effective diameter and low humidity of the summit of Mauna Kea. 261 robotic fingers keep the primary mirror in a perfect shape no matter where the telescope is pointing in the sky.

The M31 is the largest spiral galaxy in the neighbor of Milky Way and is about 770kpc away from us. Our survey expects higher event rate of PBH microlensing than the previous search, owing to the wide field-of-view and excellent image quality for the dense star field. The one pointing of HSC can cover the entire bulge and disk regions of M31. However, the analysis is expect to be not straightforward; for example, reduction procedures need some careful treatments because no previous transient search performed a careful reduction for images with such a dense field taken by highly resolved wide field camera. Thus we will develop the method to optimize the transient analysis using the software called HSC-pipe.

3. PROPERTIES OF SECURE CANDIDATES

3.1. *Properties of secure candidates*

In this section we discuss properties of secure candidates whose light curve has a typical transient feature (flash, contiguous variation, etc.), as shown in the left panel of Fig. **??**. Our classification of different types of time-variable stars is based on our eye-ball checks of their light curves. We found 11,462 secure candidates.

To study color of each secure candidate we used the g-band data of M31 that was taken in the engineering run on June 16, 2013, in addition to our r-band data. The g-band data have a seeing size of about $0.6''$, consist of 10 exposures, and have 750 seconds in total ($120 \times 5 + 30 \times 5$). We made the coadd images of the g-band data. We used Kurucz (1993) to model the stellar color taking into account the HSC filter responses we used.

In the following, we summarize properties of each type of time-variable candidates. The typical light curve for each type is shown in Fig. **??**, and the light curves for individual promising candidates are given in Appendix 3.3.

- Eclipsing binary
  This type of candidates display a light curve with eclipse dip, during a given duration, and then such a transient feature repeats with a given period. We classify these kinds of candidates as an eclipse binary of stars, where two stars are rotating around each other and either of the two stars causes an eclipse on another star, leading a dip in the light curve of their total flux. The depth of ellipse, time duration and period are different from candidate to candidate. All the candidates seem to be M-type stars based on their *g*-*r* colors. The candidates are described in Fig. 1.

- Binary stars
  For candidates that have pulsating light curves, we classify those as candidates of binary stars. If the two amplitudes of light curve within one period are similar, the stars have almost same mass and size stars. Their *g*-*r* colors indicate that almost all binary systems are M-type stars. About 10 systems have a period shorter than our observation duration (about 7 hours), and the shortest period is about 1.2 hours. These short period binary systems would be a contact binary system, where the two stars share the common envelope. These binary systems we found are shown in Fig. 2.

- Cepheid variable stars
  For candidates whose light curves display a rising or declining curve over 7 hours with about 0.1-1 magnitude change, we classify those as Cepheid variable star candidates. Most Cepheid candidates are found along the disk region of M31, and the distribution seems to match the distribution of classical δ Cep variable stars found by PAndromeda project (Kodric et al. 2013). Due to the limited time observation, we can't measure an entire period of the light curve, so can't determine the period of each candidate. Their g-r colors indicate that most candidates are A- or F-type stars. Fig. **??** show the Cepheid candidates.

- Stellar flare
  For the candidates whose light curve shows a sudden magnification in brightness, followed by an almost exponential decay, we classify the candidates as a stellar flare. The magnification is typically 1 mag, but one candidate shows almost more than 2 magnitude magnification. Their g-r colors indicate that most candidates are M-type stars. Hence, these flare stars are likely to

be in the MW halo region. Prominent star flare is a well-known phenomena for a M-type star, and originates from a reconnection of the magnetic field in the atmosphere as observed in the Sun. We didn't find a flare candidate for G-type star. This is consistent with the previous work, which shows that M-stars have more frequent flare events because energetics in the atmosphere is more affected by their magnetic field compared to G-type stars (Moffett 1974; Lacy et al. 1976; Henry & Newsom 1996).

- Moving objects: asteroids in the Solar system
These candidates are main confusion to microlensing search. These candidates display a Gaussian-shape curve at the fixed WCS position. However, after more careful look of these candidates, we found that these candidates are moving objects: point-source images in the time-sequential difference images display a clear trail in the postage-stamp image region. Hence, we consider these candidates as asteroids or comets in the Solar system. We have so far found two promising candidates of asteroids.

- Fake candidates near to the edge of CCD chip
We sometime found fake candidates that are around pixels within a few pixels from CCD chip edge. These are electrostatic effects near the edge of CCDs (a few pixels for our Hamamatsu CCDs) which means that the photometry is incorrect. This magnification feature is unique property for shot-period sampling: from the same test as discussed in § 3.1, we found that candidates from longer sampling selection are not sensitive to this incorrect photometry. One example is displayed in Appendix 3.2.

- Artificial candidates due to imperfect photometry correlated with seeing size
These are fake candidates whose light curve is as shown in Fig. **??**. Even if we identify a candidate from a PSF-like source in the difference image and then make the photometry to measure the light curve from the time-sequential difference images, the resulting light curves has a similar shape or correlation with seeing size. Hence, we conclude that this is due to an imperfect subtraction of the reference image from the target image due to the imperfect PSF measurement. Hence, we think that the light curve has a correlation with the seeing size. In particular, the exposures around ~ 3500 and $\sim 14,000$ sec have a bad seeing ($\sim 1.0''$), and the light curve shows a feature (e.g. bump or dip) around the particular epochs. When a CCD pixel has a defect, it sometimes causes an artificial image in the difference image. Furthermore, we sometime found artificial candidates in the vicinity of a bright star due to the imperfect image subtraction. After checking these images by visual inspection, we identify these fake objects. Some examples are shown in Appendix 3.2.

- Candidates whose light curve peaks at the best-seeing epochs
1,000 candidates have a similar light curve which peaks at the best-seeing epochs. The exposures of best-seeing conditions are deepest, and the PSF photometry at the candidate position has least contamination from the surrounding stars. Most candidates have a peak magnitude of $r \sim 24.5$ - 25, and the distribution of these candidates is across the halo region of M31. If these candidates are RR-Lyrae variable stars, which have an absolute magnitude of $r \sim 1$mag, the apparent magnitude is consistent with the hypothesis that the RR-Lyrae stars are in 750 kpc distance, which is the distance to M31. However, selection from color criteria of the Solar spectral models suggests that many of them are M-type or K-type stars, which is inconstant with empirical law that RR-Lyrae variables tend to be A-type or F-type stars. Still there are more than 100 candidates of A-type or F-type candidates. Note that currently we cannot distinguish these candidates from fake candidates (see the detail in § 3.1).

Following the above study we also get some indication of event properties as follows:

(1) Frequency of time variables for each type of variable stars
Our observation has unique property that many light curves has a peak $\sim$ 11000sec, around the best seeing period as displayed in Fig. **??**. To see if these peaks are real, we imposed another detection conditions as following § **??**: first separate all images into even-odd groups using serial numbers. For each group we conducted the same detection tests as mentioned before; imposing selection conditions to the each stacked images that are composed of five time-sequential images. The final time-variable candidates are constructed from those which passed the conditions more than twice. Therefore we construct two sets of candidates which can imply for the variable stars with timescale longer than 20 minutes.

We compared the two results of even-odd tests with the candidates of 10 minutes cadence, derived from § **??**. The candidates are be classified into three groups by the detection frequency and property: the first group including those detected in both even-odd cases, the second corresponding to those detected either in even-odd criteria, and the third constructed by those detected in only in previous analysis. The first group includes candidates that are feasible, most of which contain smooth curve or bumps; characteristics often seen in Cepheid stars or binary stars. Also the candidates categorized in the third group are likely to be fakes because many of them have noisy behavior or log-flux peaks. The unique event with peaks around the best seeing are contained in all three group sets, with almost the distribution for three cases. The same is true for events with sub-peaks correlated with the variation of seeing. Although we cannot get clear implications for the seeing-correlated events, this sampling rate test can work as a way to remove fake candidates.

(2) Color and magnitude property
Color and magnitude are important rulers to measure the stellar property. In this study we classify the time-variable candidates with these properties. Fig. **??** shows the results. Color selection suggest that many variable candidates have colors corresponding to low temperature stars, with similar distribution as suggested by faint star distribution. Also, most of stars in M31 disk have similar color or magnitude properties with g-$r \sim 0$.

3.2. *Effects from non-celestial moving bodies*

Short-cadence transient survey can be suffered from non-celestial causes from telescope or CCD properties. In this section we summarize the possible properties suggested from our results.

- Defraction spikes
  There are around 80 events with some sharp peaks in the light curves, which are not correlated with the time-variation of seeing. For these events many spiky patterns show up as in Fig. **??**, especially around nearby bright stars. These spikes are artificial noise of telescope, caused by the change of the targeting direction in the sky. The patterns turn clockwise around a star as the observation goes on, and magnify the surrounding stars when the spikes pass by.

- CCD edge
  In this HSC-M31 study we fixed the observational field of view by automatic tracking system of the telescope so as to reduce the coordinate uncertainty in image difference technique. However, there exists small movement due to the uncertainty of the tracking system as displayed in the lower left panel of Fig. **??**. Therefore electrostatic effects near the edge of CCDs (a few pixels for our Hamamatsu CCDs) cause incorrect photometry, which induces magnification of flux for nearby objects as in the upper left panel. Around a few hundred stars close to CCD edges are detected as candidates in our observation.

- CCD defect
  There also exist around 30 cases where small defected parts of CCD are detected as transient candidates. As CCD defects cannot give correct flux measurement, they sometimes produces small bright region in difference images, which are detected as time-variant candidates.

3.3. *Characteristics of unique events*

In this section we describe some detailed properties of unique candidates.

3.3.1. *Eclipsing binary stars: white - brown dwarf system*

Among the eclipsing binaries we found a unique candidate; as shown in Fig, **??**, one dark star totally hide the other star so that the flux becomes totally dark. This system is considered to be composed by a white dwarf and a brown dwarf.

3.3.2. *A star before nova*

A red nova was found on February 2015, about three months after our observation. Therefore the candidate might be at the stage of merging of two stars. Fig. **??** shows the light curve and image of the target star, at 00h 42m 07.99s +40d 55m 01.1s in radec coordinate which is close to M31 bulge. This object is not detected with our selection criteria probably due to small change of flux. The magnification is only 0.02 mag during our observation, which is so small that we cannot say clearly if this is true.

3.3.3. *Appearing star or disappearing star*

There are around 10 stars which suddenly appear or disappear during observation without the effect from CCD edge. We could not find out the reason so far, but many of them reside close to the bulge region.

4. SUMMARY AND CONCLUSION

In this work we discussed our tests of nature of dark matter on star scales, and searched dark matter candidate so-called primordial black hole (PBH). We make use of microlensing effect for the search which is expected when PBH comes in the line of sight of background stars. Microlensing effect is rare event; only one in million stars can happen. Thus we used the Hyper Suprime-Cam (HSC) images of Andromeda Galaxy (M31) on stars in M31 to gather large number of stars and achieve higher event rate. The PBH is one of viable candidates for dark matter, and we performed tests to establish a way to constrain the abundance of PBHs of mass scales, 10^{-9}-$10^{-7} M_{\odot}$, with the dense-cadence imaging data from wide-field camera. One large problem is that default analysis mode of HSC-pipe software could not reduce the images with large number of stars; which caused troubles as in background subtraction, star catalog construction, image difference, and event detection. Therefore we managed to establish the reduction method as described in § 3 and § **??**, to extract transient candidates from the images.

From the reduced images we performed two kinds of analysis: transient study and microlensing implication. As for transient study we succeeded to extract as much as $\sim 11,000$ transient candidates. We draw light curves for all the events and classified them by peak characteristics, *g*-*r* color and magnitude. These characteristics help us figure out unique candidates as well as noise properties. The summary of candidate characteristics is provided in § **??** and Appendix 3.2 and 3.3. We also started the second analysis; estimating microlensing properties and implication expected from our data. Currently we could not find any microlensing candidates from the data by the fitting of theoretical microlensing light curve. Thus we started to estimate the upper limit of mass fraction of PBH to the total dark matter abundance implicated from our data. As our data covers large field of view, we need to take into account field-dependent properties such as star number counts and extinction. Therefore we divided the field of view into 10×10 sub-regions. In the first step we carefully looked into one single patch targeting region (patch=2,6) to reveal the position dependence, somehow succeeded to estimate the star number counts in the field. Our method constructed for one patch can be basically applied for wider field survey simply by considering position dependence and repeating the analysis. Also we make sure that our observation achieves strongest constraint on the mass fraction by simplified analysis.

This project is still ongoing, and we might need further investigation of microlensing property. Especially disk and bulge region we might need further correction for estimating the magnitude or number counts of stars, because peak counts might not work for these regions. Also for microlensing event from PBHs in M31 halo region, we need to estimate the event rate more carefully by taking into account so-called finite-source effects or limb-darkening effect, which might greatly affect event time-scale estimation (see Riffeser et al. 2008, for the detail).

The development achieved in our study can be applied to to future new time-space astronomy; aiming at faint, short-timescale events by wide-field or short-cadence survey. Currently several wide-field deep transient surveys are ongoing or planned not only by HSC, but also by the Palomar Transient Factory (PTF)[1] and the Large Synoptic Survey Tele-

[1] http://www.ptf.caltech.edu/iptf

scope (LSST)[2]. As for transient candidates, we can establish clear criteria to categorize the events like flares and binary stars including noise characteristics. Since our observation presents unique properties of faint, short-timescale variable candidates that has never been searched before, it would be helpful to characterize the time-dependent behavior of events in the future short cadence survey; as for microlensing study, event criteria can work as reference to remove contamination from microlensing candidates, for example.

ACKNOWLEDGMENTS

MT was supported by World Premier International Research Center Initiative (WPI Initiative), MEXT, Japan, by the FIRST program "Subaru Measurements of Images and Redshifts (SuMIRe)", CSTP, Japan. MT was supported by Grant-in-Aid for Scientific Research from the JSPS Promotion of Science (No. 23340061 and 26610058).

REFERENCES

Henry, G. W., & Newsom, M. S. 1996, PASP, 108, 242
Kodric, M., et al. 2013, AJ, 145, 106
Kurucz, R. L. 1993, VizieR Online Data Catalog, 6039
Lacy, C. H., Moffett, T. J., & Evans, D. S. 1976, ApJS, 30, 85
Moffett, T. J. 1974, ApJS, 29, 1
Riffeser, A., Seitz, S., & Bender, R. 2008, ApJ, 684, 1093

[2] http://www.lsst.org

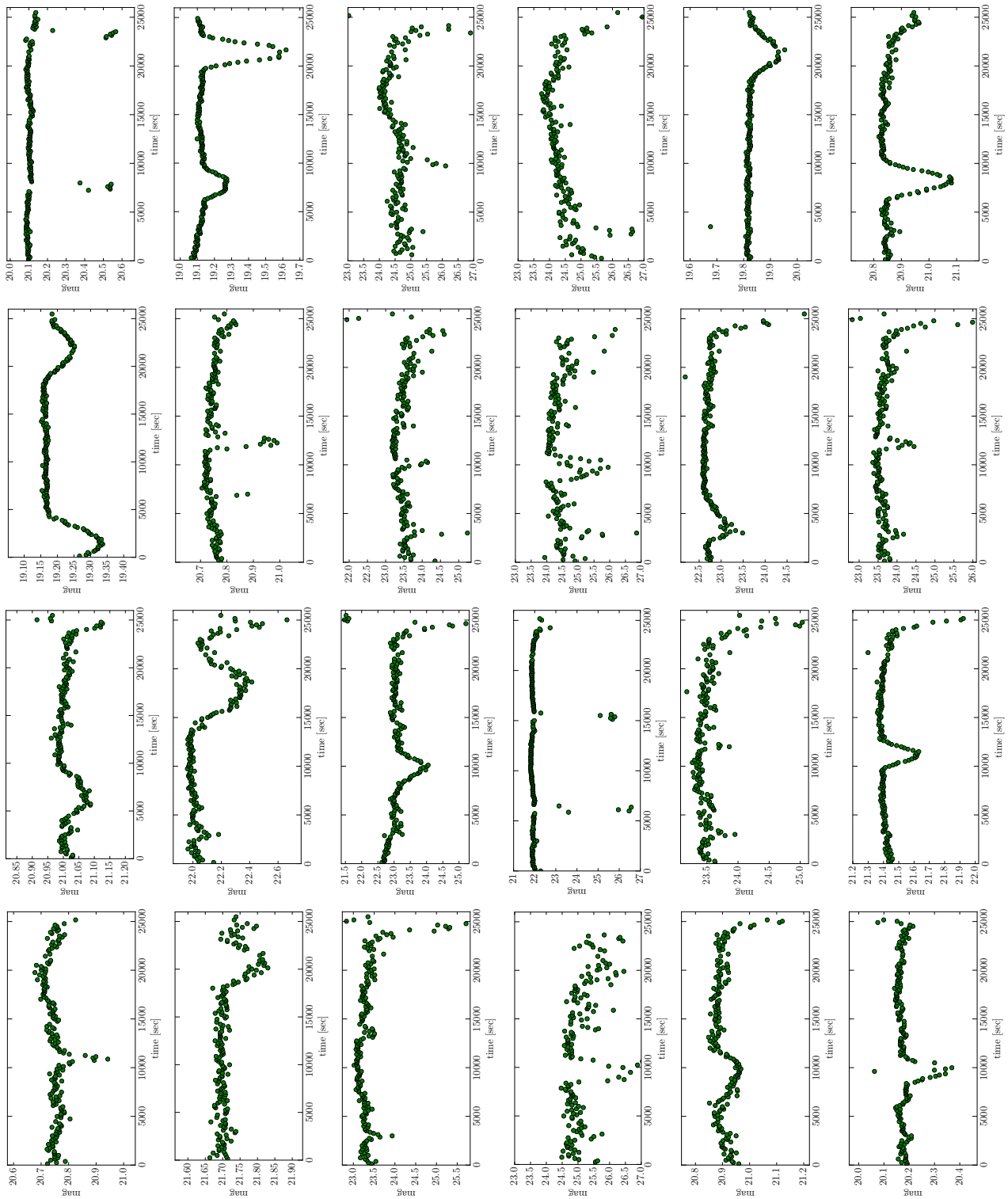

Figure 1. Light curves of eclipsing binary-star candidates.

Table 1
Coordinates of eclipsing-binary stars

RA	DEC	m_r	g-r	color flexibility
00:46:23.367436	40:54:41.021361	18.98	1.36	0.5
00:46:03.819192	40:53:24.470028	23.51	1.21	0.6
00:46:35.415323	41:23:31.458501	24.85	1.04	~ 1.5
00:45:51.658176	41:32:55.861792	24.09	0.62	~ 2.0
00:45:05.353110	40:59:47.805878	20.05	0.89	0.45
00:44:44.277844	40:44:30.562548	19.81	0.62	0.12
00:44:00.778958	40:54:01.372526	20.84	1.50	0.25
00:44:27.792024	41:07:56.697349	23.52	0.89	0.4
00:42:54.977624	40:33:51.532856	19.17	0.69	0.18
00:42:06.658803	40:45:26.010669	20.74	1.15	0.28
00:41:58.545704	40:59:11.430024	23.27	0.45	<0.6
00:41:55.943126	41:45:24.764765	24.34	0.99	~ 2.0
00:41:26.646108	41:07:45.671123	22.60	1.54	0.5
00:41:23.452798	41:02:57.356847	23.65	1.32	~ 1.5
00:41:30.525136	41:12:12.865234	23.42	0.28	1.2
00:41:00.841712	41:16:11.965934	20.98	1.50	0.07
00:40:53.075820	41:38:40.521759	21.99	1.32	0.4
00:40:30.829483	40:49:52.136096	22.90	0.04	1.0
00:40:00.350583	40:57:36.530184	21.84	0.40	~ 5.0
00:40:37.983087	41:57:12.621315	22.34	0.86	0.24
00:39:17.466419	41:23:19.579930	21.40	1.44	0.2
00:39:37.446521	41:42:57.151766	20.39	1.25	0.2
00:38:42.901297	41:15:11.594215	21.70	1.46	0.14

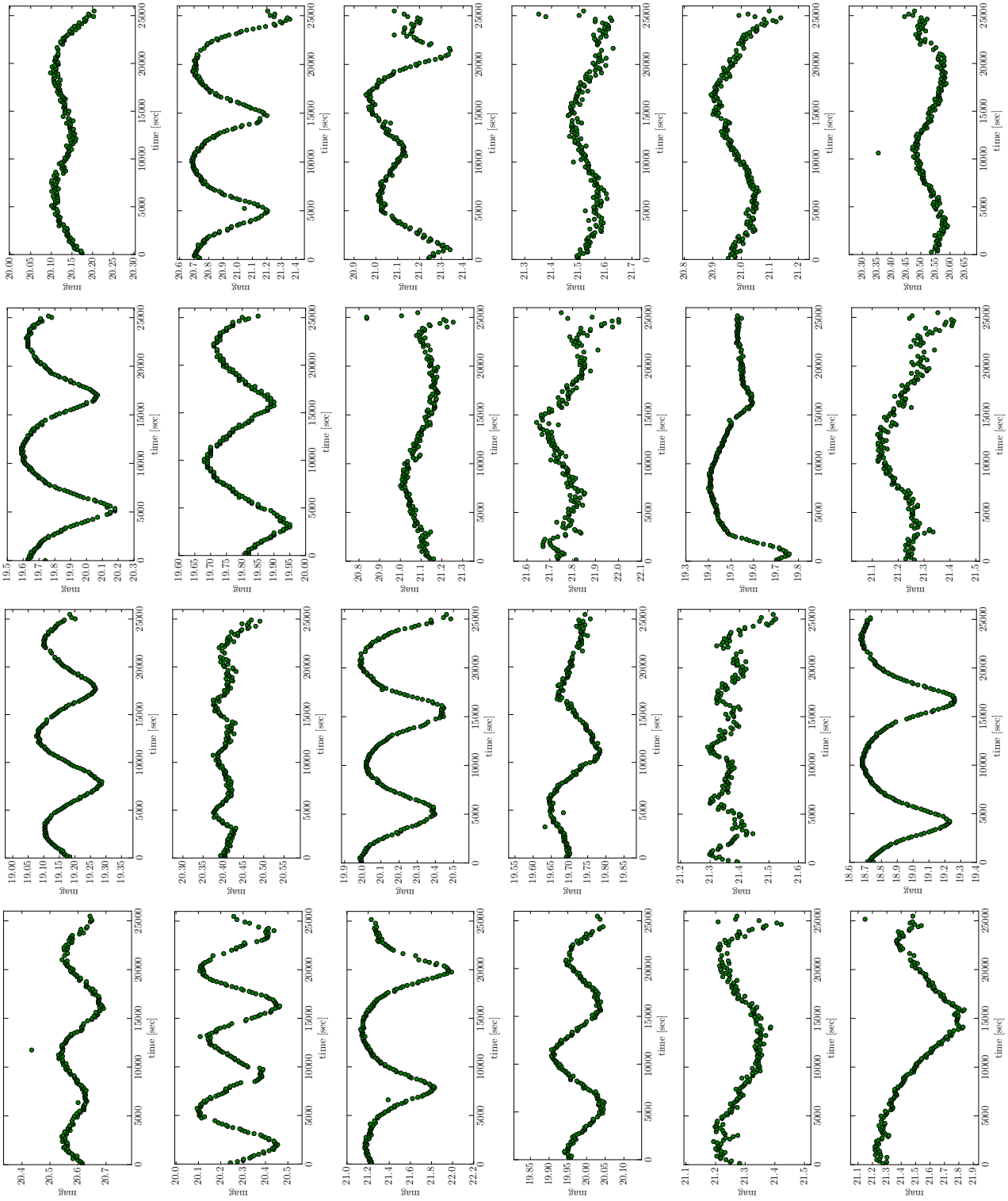

Figure 2. Light curves of binary-star candidates.

Table 2
Coordinates of binary stars

RA	DEC	m_r	g-r	color flexibility
00:45:26.7342	41:26:23.9275	20.74	0.88	0.5
00:45:22.1774	41:24:17.6419	21.12	1.09	0.4
00:38:45.4971	41:26:33.6937	19.92	0.97	0.15
00:38:48.7594	41:21:50.6669	21.16	0.46	0.8
00:38:50.7255	41:19:45.9761	21.49	1.24	0.4
00:39:16.4262	41:29:02.6488	21.40	0.85	0.18
00:39:50.2571	40:51:22.6766	19.52	0.77	0.6
00:40:24.3784	41:04:03.3898	21.33	0.06	0.1
00:41:14.4559	41:45:06.7162	19.78	1.37	0.18
00:41:44.3328	40:36:36.8813	20.05	0.78	0.4
00:42:26.4405	41:55:09.3537	20.39	0.35	0.05
00:42:11.4126	41:32:31.7261	19.13	0.69	0.2
00:42:59.1865	41:56:09.6229	19.45	1.28	0.35
00:43:35.1125	41:24:07.6338	21.72	0.20	0.15
00:43:42.4663	41:23:57.7301	21.06	0.13	0.15
00:43:42.3203	40:53:24.0968	19.69	0.69	0.3
00:44:19.4817	41:40:26.4706	19.57	0.80	0.87
00:44:20.7171	41:35:34.6790	20.89	-0.04	0.05
00:44:43.2779	41:43:18.2840	20.48	0.58	0.15
00:44:08.0240	41:32:54.4263	20.98	-0.18	0.15
00:44:48.8823	41:33:30.4398	21.51	-0.08	0.15
00:45:29.5286	41:43:56.6457	21.11	0.10	0.3
00:45:49.070	41:04:20.7016	20.15	0.73	> 0.1
00:41:48.197	40:52:14.1655	22.45	-0.48	> 0.6
00:42:47.366	41:32:54.8839	22.52	-0.38	> 0.4
00:42:07.135	41:01:28.9674	21.13	0.01	> 0.2
00:45:05.220	41:38:46.3025	21.02	0.20	> 1.0
00:43:42.739	40:49:22.9928	23.65	-0.17	> 2.0
00:39:45.031	40:51:46.4835	21.26	0.02	> 0.2
00:43:44.989	41:23:04.2061	22.80	-0.65	> 1.0

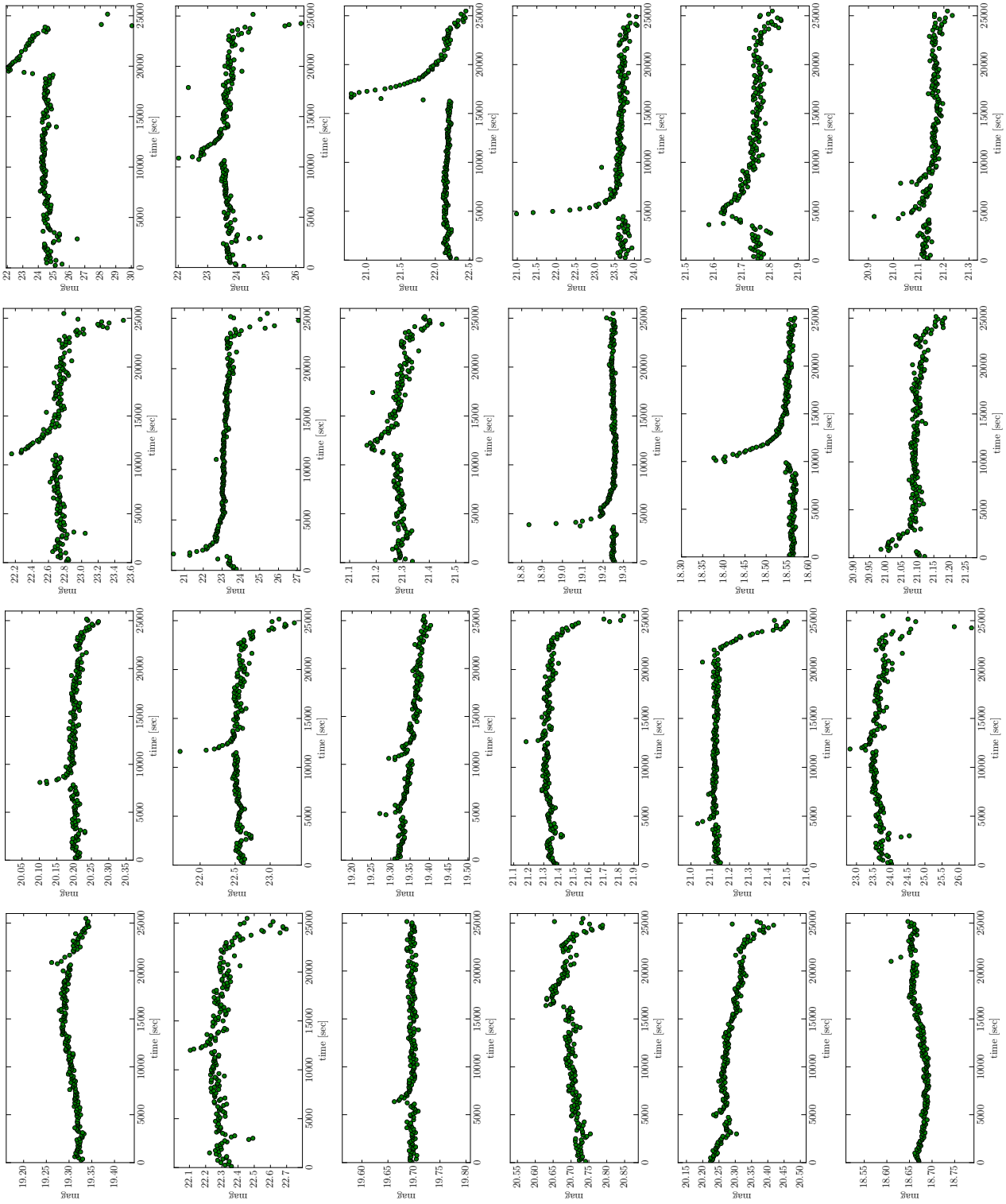

Figure 3. Light curves of flare-star candidates.

Table 3
Coordinates of flare stars

RA	DEC	m_r	g-r
00:44:18.16631	41:55:38.9326	19.68	1.29
00:43:52.21989	41:23:18.4119	21.31	1.35
00:39:16.38949	41:21:26.0948	18.55	1.38
00:39:21.39091	41:12:08.2521	21.16	1.48
00:39:19.34802	40:52:00.5147	22.72	0.70
00:40:12.90790	41:17:37.6416	21.09	1.41
00:40:38.65823	41:08:56.3901	22.21	1.55
00:41:09.5941	41:35:00.0181	20.22	1.19
00:41:47.59828	41:26:31.7830	23.03	1.95
00:42:03.5380	41:34:57.6109	23.36	1.57
00:42:30.20150	41:49:38.3266	22.51	1.56
00:42:06.99683	41:45:51:5045	23.62	1.65
00:45:40.10468	41:40:36.1484	20.69	1.39
00:45:12/30174	41:09:31.3176	24.27	2.33
00:44:56.85637	40:51:53.0574	19.32	1.50
00:45:15.34176	40:44:28.4274	21.75	1.53
00:45:34.32083	40:42:37.8898	23.60	1.83
00:46:09.89194	41:23:49.7838	22.17	1.25
00:43:40.82533	41:54:34.5093	21.25	0.37
00:42:59.31124	41:35:33.2675	20.26	1.30
00:44:00.12399	40:39:34.4537	19.28	1.77
00:46:30.55432	40:59:39.3800	21.14	1.76
00:40:23.08478	41:37:25.1962	19.15	1.10
00:41:19.24417	41:47:35.3886	21.44	1.40
00:42:56.89261	40:53:25.2952	20.49	1.35
00:42:17.73107	41:53:47.5167	18.69	1.41
00:46:03.28415	41:05:39.6373	19.31	1.24
00:40:45.80663	41:38:15.1071	21.44	1.47
00:39:25.79447	40:50:46.5293	21.56	0.67
00:44:32.1359	41:18:43.8608	21.02	0.96